A 3D tunable and multi-frequency graphene plasmonic cloak

Mohamed Farhat,[1,*] Carsten Rockstuhl,[2] and Hakan Bağcı[1]

[1]*Division of Computer, Electrical, and Mathematical Sciences and Engineering 4700 King Abdullah University of Science and Technology Thuwal 23955-6900, Saudi Arabia*
[2]*Institute of Condensed Matter Theory and Solid State Optics, Abbe Center of Photonics, Friedrich-Schiller-Universität Jena, Max-Wien-Platz 1, D-07743 Jena, Germany*
[*]*mohamed.farhat@kaust.edu.sa*

Abstract: We demonstrate the possibility of cloaking three-dimensional objects at multi-frequencies in the far-infrared part of the spectrum. The proposed cloaking mechanism exploits graphene layers wrapped around the object to be concealed. Graphene layers are doped via a variable external voltage difference permitting continuous tuning of the cloaking frequencies. Particularly, two configurations are investigated: (i) Only one graphene layer is used to suppress the scattering from a dielectric sphere. (ii) Several of these layers biased at different gate voltages are used to achieve a multi-frequency cloak. These frequencies can be set independently. The proposed cloak's functionality is verified by near- and far-field computations. By considering geometry and material parameters that are realizable by practical experiments, we contribute to the development of graphene based plasmonic applications that may find use in disruptive photonic technologies.

OCIS codes: (230.3205) Invisibility cloaks; (160.3918) Metamaterials; (050.6624) Subwavelength structures.

References and links

1. J. B. Pendry, D. Schurig, and D. R. Smith, "Controlling electromagnetic fields," Science **312**(5781), 1780–1782 (2006).
2. U. Leonhardt, "Optical conformal mapping," Science **312**(5781), 1777–1780 (2006).
3. T. Ergin, N. Stenger, P. Brenner, J. B. Pendry, and M. Wegener, "Three-dimensional invisibility cloak at optical wavelengths," Science **328**(5976), 337–339 (2010).
4. W. Cai, U. K. Chettiar, A. V. Kildishev, and V. M. Shalaev, "Optical cloaking with metamaterials," Nat. Photonics **1**(4), 224–227 (2007).
5. M. Farhat, S. Guenneau, A. B. Movchan, and S. Enoch, "Achieving invisibility over a finite range of frequencies," Opt. Express **16**(8), 5656–5661 (2008).
6. I. I. Smolyaninov, V. N. Smolyaninova, A. V. Kildishev, and V. M. Shalaev, "Anisotropic metamaterials emulated by tapered waveguides: Application to optical cloaking," Phys. Rev. Lett. **102**(21), 213901 (2009).
7. D. Schurig, J. J. Mock, B. J. Justice, S. A. Cummer, J. B. Pendry, A. F. Starr, and D. R. Smith, "Metamaterial electromagnetic cloak at microwave frequencies," Science **314**(5801), 977–980 (2006).
8. A. Alù and N. Engheta, "Achieving transparency with plasmonic and metamaterial coatings," Phys. Rev. E Stat. Nonlin. Soft Matter Phys. **72**(1), 016623 (2005).
9. A. Alù and N. Engheta, "Plasmonic materials in transparency and cloaking problems: Mechanism, robustness, and physical insights," Opt. Express **15**(6), 3318–3332 (2007).
10. S. Mühlig, M. Farhat, C. Rockstuhl, and F. Lederer, "Cloaking dielectric spherical objects by a shell of metallic nanoparticles," Phys. Rev. B **83**(19), 195116 (2011).
11. M. Farhat, S. Mühlig, C. Rockstuhl, and F. Lederer, "Scattering cancellation of the magnetic dipole field from macroscopic spheres," Opt. Express **20**(13), 13896–13906 (2012).
12. D. Rainwater, A. Kerkhoff, K. Melin, J. C. Soric, G. Moreno, and A. Alù, "Experimental verification of three dimensional plasmonic cloaking in free-space," New J. Phys. **14**(1), 013054 (2012).
13. K. S. Novoselov, A. K. Geim, S. V. Morozov, D. Jiang, Y. Zhang, S. V. Dubonos, I. V. Grigorieva, and A. A. Firsov, "Electric field effect in atomically thin carbon films," Science **306**(5696), 666–669 (2004).
14. A. H. Castro Neto, F. Guinea, N. M. R. Peres, K. S. Novoselov, and A. K. Geim, "The electronic properties of graphene," Rev. Mod. Phys. **81**(1), 109–162 (2009).

15. R. R. Nair, P. Blake, A. N. Grigorenko, K. S. Novoselov, T. J. Booth, T. Stauber, N. M. R. Peres, and A. K. Geim, "Fine structure constant defines visual transparency of graphene," Science **320**(5881), 1308–1308 (2008).
16. K. S. Novoselov, V. I. Fal'ko, L. Colombo, P. R. Gellert, M. G. Schwab, and K. Kim, "A roadmap for graphene," Nature **490**(7419), 192–200 (2012).
17. T. Mueller, F. N. Xia, and P. Avouris, "Graphene photodetectors for high-speed optical communications," Nat. Photonics **4**(5), 297–301 (2010).
18. M. Liu, X. Yin, E. Ulin-Avila, B. Geng, T. Zentgraf, L. Ju, F. Wang, and X. Zhang, "A graphene-based broadband optical modulator," Nature **474**(7349), 64–67 (2011).
19. E. H. Hwang and S. Das Sarma, "Dielectric function, screening, and plasmons in two-dimensional graphene," Phys. Rev. B **75**(20), 205418 (2007).
20. M. Jablan, H. Buljan, and M. Soljacic, "Plasmonics in graphene at infrared frequencies," Phys. Rev. B **80**(24), 245435 (2009).
21. L. Ju, B. Geng, J. Horng, C. Girit, M. Martin, Z. Hao, H. A. Bechtel, X. Liang, A. Zettl, Y. R. Shen, and F. Wang, "Graphene plasmonics for tunable terahertz metamaterials," Nat. Nanotechnol. **6**(10), 630–634 (2011).
22. F. H. L. Koppens, D. E. Chang, and F. J. García de Abajo, "Graphene plasmonics: A platform for strong light-matter interactions," Nano Lett. **11**(8), 3370–3377 (2011).
23. L. Wang, W. Cai, X. Zhang, and J. Xu, "Surface plasmons at the interface between graphene and Kerr-type nonlinear media," Opt. Lett. **37**(13), 2730–2732 (2012).
24. K. Y. Shin, J.-Y. Hong, and J. Jang, "Micropatterning of graphene sheets by inkjet printing and its wideband dipole-antenna application," Adv. Mater. **23**(18), 2113–2118 (2011).
25. J. Christensen, A. Manjavacas, S. Thongrattanasiri, F. H. L. Koppens, and F. J. García de Abajo, "Graphene plasmon waveguiding and hybridization in individual and paired nanoribbons," ACS Nano **6**(1), 431–440 (2012).
26. A. Vakil and N. Engheta, "Transformation optics using graphene," Science **332**(6035), 1291–1294 (2011).
27. P.-Y. Chen and A. Alù, "Atomically thin surface cloak using graphene monolayers," ACS Nano **5**(7), 5855–5863 (2011).
28. S. Thongrattanasiri, F. H. L. Koppens, and F. J. García de Abajo, "Complete optical absorption in periodically patterned graphene," Phys. Rev. Lett. **108**(4), 047401 (2012).
29. A. Yu. Nikitin, F. Guinea, F. J. Garcia-Vidal, and L. Martin-Moreno, "Fields radiated by a nanoemitter in a graphene sheet," Phys. Rev. B **84**(19), 195446 (2011).
30. R. Alaee, M. Farhat, C. Rockstuhl, and F. Lederer, "A perfect absorber made of a graphene micro-ribbon metamaterial," Opt. Express **20**(27), 28017–28024 (2012).
31. J. W. Ko, S.-W. Kim, J. Hong, K. Kang, and C. B. Park, "Synthesis of graphene-wrapped CuO hybrid materials by CO2 mineralization," Green Chem. **14**(9), 2391–2394 (2012).
32. J. S. Lee, K. H. You, and C. B. Park, "Highly photoactive, low bandgap TiO2 nanoparticles wrapped by graphene," Adv. Mater. **24**(8), 1084–1088 (2012).
33. A. Alù and N. Engheta, "Cloaked near-field scanning optical microscope tip for noninvasive near-field imaging," Phys. Rev. Lett. **105**(26), 263906 (2010).
34. G. W. Hanson, "Dyadic Green's functions and guided surface waves on graphene," J. Appl. Phys. **103**, 064302 (2006).
35. P. Y. Chen, J. Soric, and A. Alù, "Invisibility and cloaking based on scattering cancellation," Adv. Mater. **24**(44), OP281–OP304 (2012).
36. P. Y. Chen and A. Alù, "Mantle cloaking using thin patterned metasurfaces," Phys. Rev. B **84**(20), 205110 (2011).
37. A. Alù, "Mantle cloak: Invisibility induced by a surface," Phys. Rev. B **80**(24), 245115 (2009).
38. F. Monticone, C. Argyropoulos, and A. Alù, "Layered plasmonic cloaks to tailor the optical scattering at the nanoscale," Sci Rep **2**, 912–918 (2012).

1. Introduction

Cloaking is undoubtedly among the most intriguing applications of metamaterials [1,2]. Recent technological advancements in manufacturing and characterizing materials at the milli-, micro-, and nano-meter scales suggest that practical cloaking will be possible in the near future [3]. The idea of cloaking exploiting transformation optics was introduced by Pendry [1]. This type of cloaking makes use of a singular transformation to predict material properties that make the cloaking region look like a point to external observers [1]. At the same time and independently, Leonhardt proposed a similar concept termed conformal invisibility, which is valid in the geometric optics limit [2]. It is now well known that this class of cloaks suffers from highly anisotropic and singular material properties required by the transformation. Particularly, the (approximate) practical numerical and experimental realizations of these singular material properties alter the ideal cloaking efficiency [4–6]. Additionally, the size of the cloaking shell is usually in the order of the object being

concealed [7]. This limits the number of possible applications since compactness is typically required for several practical uses of invisibility cloaks, such as concealing probes and sensors.

In the same vein, Alù and Engheta proposed a transparency device that exploits the scattering cancellation technique (SCT) [8]. SCT makes use of a negative local polarizability cover with low or negative permittivity to suppress the total electric dipole moment of the object being concealed. This class of cloaks has been shown to be quite robust to changes in the geometry of objects and the frequency of operation [9–11]. A recent experimental validation of SCT has been realized at microwave frequencies [12]. Like its transformation optics-based counterpart, this class of cloaks suffers from several practical physical limitations: Plasmonic cloaks have narrow band of operation since they rely on the plasmonic properties of their building blocks, which are generally noble metals with negative or close-to-zero permittivity. Once the geometry of the shell is designed and constructed, the scattering reduction is only operational at a single frequency. Practical applications would often necessitate more flexibility of the design and frequency band of operation.

In this work, to alleviate the severity of these practical implementation issues, we propose to use graphene to construct plasmonic SCT-based invisibility shells. Graphene sheets comprising honeycomb crystal of carbon atoms [sketched in Fig. 1(a)] were first isolated by Geim and Novoselov [13]. Further experimental investigations have demonstrated graphene's unusual characteristics [14–18]. Among those, the one that is most relevant to plasmonics is its ability to support the propagation of guided surface electromagnetic waves at its interface with an insulator, the so-called surface plasmon polaritons (SPPs) [19–20]. These SPPs are highly tunable through chemical doping or an external voltage difference applied to the graphene layer. Additionally, when compared to their metallic counterparts, graphene SPPs have longer propagation lengths [21]. These properties open the way for tunable plasmonics [21–23] that could have many real world applications [24–30].

In this work, the dynamically tunable SPPs induced on graphene layer(s) are exploited to circumvent some of the limitations associated with plasmonic SCT-based cloaks. The proposed cloak makes use of graphene layers wrapped around dielectric core objects to suppress their scattering response. The tunability of the scattering cancellation is achieved by biasing the graphene layers with a variable external voltage difference. Particularly, two configurations are investigated: (i) Only one graphene layer is used to conceal the scattering from a dielectric sphere. (ii) Several of these layers biased at different voltages are used to generate plasmonic cloaking at tunable multi-frequencies.

The remainder of the paper is organized as follows. First, plasmonic properties of graphene layers on top of dielectrics are analyzed to demonstrate the potential of tuning the plasmon resonance at will by sweeping the chemical potential via applying gate voltage. Then, it is demonstrated that a single layer of graphene covering a dielectric sphere can drastically reduce its scattering cross section. The dependence of the cloaking dip on the chemical potential of graphene is clearly shown. This permits the design of a tunable plasmonic cloak. This design is further developed by cascading graphene layers with gate voltages set at different levels on top of the very same obstacle. This improved cloak has multi-frequency bands of operation, i.e., many dips in the scattering cross section are observed. The number of these dips is equal to the number of layers constituting the cloak.

It should be noted here that even though only numerical experiments are provided, the proposed cloaks can actually be constructed thanks to the recent experimental progress in wrapping graphene sheets around various shapes (cylindrical or spherical) [31,32]. Additionally, it should be mentioned here that the approach to cancel the scattered fields at various frequencies proposed here may also represent a viable way for non-invasive sensing and probing with improved bandwidth [33].

2. Tunable plasmonics induced by graphene
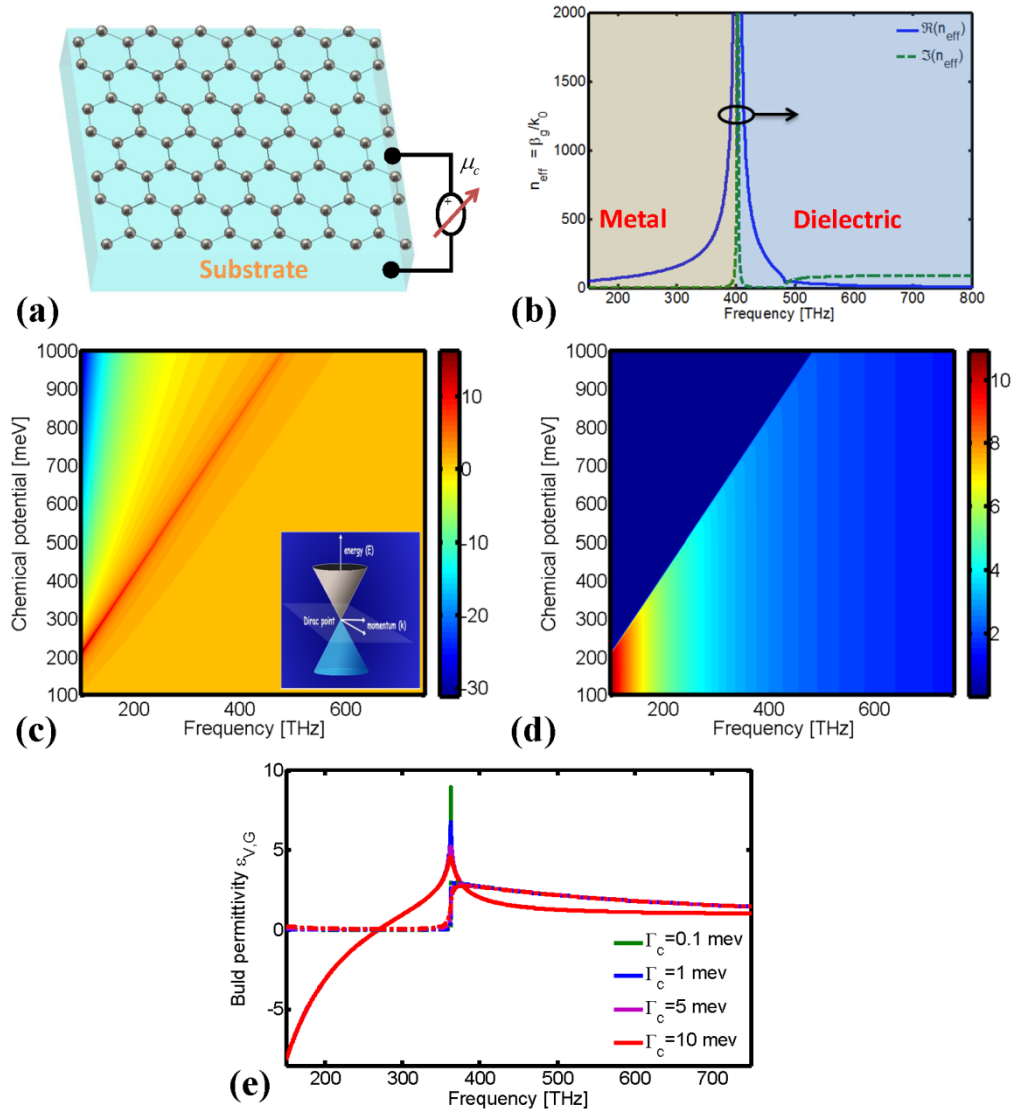
Fig. 1. (a) Sketch of a graphene sheet on top of dielectric substrate. (b) SPP dispersion relation with chemical potential set to 1000 meV. (c) Real and (d) imaginary parts of the bulk permittivity of graphene layer given by Eqs. (1)-(4) for various values of chemical potential ranging from 100 to 1000 meV and frequency ranging from 100 to 750 THz. The inset shows the energy bands of the graphene. (c) Effect of damping frequency (Γ_c) on graphene permittivity $\varepsilon_{V,G}$: solid lines represent the real part whereas dotted-dashed lines represent imaginary part.

As shown by both theoretical and experimental studies, non-doped graphene exhibits a very high absorption [15,16] at optical frequencies at zero temperatures. This is especially remarkable given the fact that thickness of a graphene layer is only sub nanometer. It should be noted here that the graphene layer's conductivity is independent of any material parameters and is only function of the fine structure constant [15]. This is mainly due to the linear dispersion relation of its quasi-particles close to the Fermi energy [inset of Fig. 1(c)]. Another important feature of graphene is its anomalous band structure: the valence band has a

negative energy whereas the conduction band has a positive energy, and both bands have an intersection point at zero energy, without any bandgap (in contrast to metals and dielectrics) [inset of Fig. 1(c)]. Graphene could thus be considered as a semiconductor with zero-gap. In contrast, doped graphene (non-zero Fermi energy or chemical potential) layers exhibit a completely different behavior: The complex surface conductivity $\sigma_{S,G}$ for a graphene layer can be calculated from Kubo's formula having contributions from intraband and interband absorption [34]:

$$\sigma_{S,G}(\omega) = \sigma_{S,G}{}'(\omega) - j\sigma_{S,G}{}''(\omega) = \sigma_{intra}(\omega) + \sigma_{inter}(\omega). \tag{1}$$

In Eq. (1), σ_{intra} and σ_{inter} represent absorption due to intraband electron-photon scattering and interband electron transition processes, respectively. They are evaluated using

$$\sigma_{intra}(\omega) = j\frac{q^2}{\pi\hbar(\hbar\omega + j\Gamma_c)}\left[\mu_c + 2k_B T \ln\left(e^{-\mu_c/k_B T} + 1\right)\right], \tag{2}$$

$$\sigma_{inter}(\omega) = j\frac{q^2}{4\pi\hbar}\ln\left[\frac{2|\mu_c| - (\hbar\omega + j\Gamma_c)}{2|\mu_c| + (\hbar\omega + j\Gamma_c)}\right], \tag{3}$$

respectively. It should be noted here that the second expression is simplified and valid in the regime where $|\mu_c|, \hbar\omega \gg k_B T$. Here, ω is the angular frequency, q is the charge of electron, $\hbar$ is the reduced planck constant, k_B is the Boltzman constant, T is the temperature, μ_c is the chemical potential of doped graphene layer, and Γ_c is the damping constant. The temperature is assigned the default value of $T = 300\,\text{K}$. The damping constant of graphene reads as $\Gamma_c = q\hbar v_f{}^2/\mu\mu_c$, where $v_f = c/300\,\text{m/s}$ is the Fermi velocity, $\mu = 10,000\,\text{cm}^2/Vs$ is the electron mobility. Note that this choice of μ is a rather conservative upon considering latest experimental results provided in [16]. As could be seen from Eqs. (2) and (3) both the interband and intraband absorption are dependent upon the chemical potential μ_c, damping Γ_c and operating frequency ω.

It is assumed here that graphene layer has a very small thickness δ in comparison to wavelength of excitation. Under this assumption bulk conductivity $\sigma_{V,G}$ and surface conductivity $\sigma_{S,G}$ are related accurately with the equation $\sigma_{V,G} = \sigma_{S,G}/\delta$. Using Ohm's and static Ampere's laws, one may obtain the expression of the relative bulk permittivity:

$$\varepsilon_{V,G}(\omega) = 1 + j\sigma_{V,G}(\omega)/\varepsilon_0\omega. \tag{4}$$

Graphene layers with complex permittivity $\varepsilon_{V,G}$ given by Eq. (4) support SPPs on the interfaces with dielectrics. The propagation constant associated with this SPP, β_g, follows the dispersion relation $\beta_g = k_0\sqrt{1 - (2/\eta_0\sigma_{S,G})^2}$, where k_0 and η_0 are the wavenumber and wave impedance in free-space, respectively. This SPP is responsible for the unusual plasmonic properties of the graphene. The effective index corresponding to this SPP is shown in Fig. 1(b). This figure demonstrates the dual behavior of the graphene layer: At low frequencies it behaves like a metal whereas at higher frequencies it has the properties of a dielectric. The frequency of metal-dielectric transition depends on the chemical potential μ_c. It should also be noted here that the value of effective index is very high compared to noble

metals, which results in stronger confinement of light and enhanced subwavelength coupling to matter.

The dependence of the complex permittivity of graphene, $\varepsilon_{V,G}$ given by Eq. (4), on the chemical potential μ_c and the damping coefficient Γ_c parameters is characterized between 100 and 800 THz. Figures 1(c) and 1(d) plot real and imaginary parts of $\varepsilon_{V,G}$ as a function of chemical potential μ_c and frequency. They clearly show the resulting blue-shift as μ_c is increased at a given frequency. Figure 1(e) characterizes the effect of damping Γ_c for a fixed value of μ_c and clearly demonstrates the decreasing and broadening of $\varepsilon_{V,G}$ around the metal-dielectric transition frequency when Γ_c is increased. As demonstrated in Fig. 1, the optical properties of graphene could be largely controlled by its chemical potential μ_c and damping coefficient Γ_c. Note that Γ_c depends on the purity of graphene sheets and the experimental method used to produce it, whereas μ_c can be easily tuned via doping or applying a gate voltage V_g. The latter is preferred here since it makes it possible to dynamically tune the variation in the far-infrared response of the graphene SPPs. This is not possible with conventional noble metals (e.g. gold and silver). This key characteristic of graphene is exploited in the plasmonic SCT-based cloak designs to achieve a tunable frequency response and multi-frequency band of operation as detailed in the following two sections.

It should be noted here that in the simulations carried out for this work, the thickness of the graphene layer $\delta = 1\,\text{nm}$. This choice was mainly motivated by the seminal work of Vakil and Engheta [26] and several others studying graphene plasmonics [22]. As expected, the actual value of δ, provided that it is much smaller than the wavelength of excitation, has a negligible impact on the optical response of the designs under study.

3. Dynamically tunable plasmonic SCT-based cloak

3.1 Tunable single layered cloak

Let a subwavelength spherical nanoparticle of radius a with relative permittivity ε represent the object to be concealed. The object is covered by a graphene shell of outer radius a_c with relative permittivity $\varepsilon_{V,G}$. Note that the difference between the inner and outer radii of the graphene shell is equal to δ, i.e., the thickness of the graphene layer. The whole structure is assumed to be centered at the origin of a spherical coordinate system without loss of generality. The structure is excited with a time harmonic electromagnetic plane wave with time variation $e^{-j\omega t}$. It has been shown in [9] that the scattering cross section, σ_S, of the structure can be expressed in terms of electric and magnetic multipole coefficients, c_n^{TE} and c_n^{TM}. Here, n is the order of the multipole expansion. The coefficients c_n^{TE} and c_n^{TM} relate scattered and incident fields and are functions of the object's geometry and the frequency of the excitation ω. Their expressions are obtained from the continuity relations at the boundaries between different layers of the whole object [35,36]

$$c_n^{\text{TE,TM}}(\omega) = -\frac{U_n^{\text{TE,TM}}(\omega)}{U_n^{\text{TE,TM}}(\omega) + jV_n^{\text{TE,TM}}(\omega)}. \qquad (5)$$

Here, the determinant U_n^{TM} associated with the nth magnetic multipole coefficient is given by [9]:

$$U_n^{\mathrm{TM}}(\omega) = \begin{vmatrix} j_n(ka) & j_n(k_c a) & y_n(k_c a) & 0 \\ j_n'(ka)/\varepsilon & j_n'(k_c a)/\varepsilon_{\mathrm{V,G}}(\omega) & y_n'(k_c a)/\varepsilon_{\mathrm{V,G}}(\omega) & 0 \\ 0 & j_n(k_c a_c) & y_n(k_c a_c) & j_n(k_0 a_c) \\ 0 & j_n'(k_c a_c)/\varepsilon_{\mathrm{V,G}}(\omega) & y_n'(k_c a_c)/\varepsilon_{\mathrm{V,G}}(\omega) & j_n'(k_0 a_c)/\varepsilon_0 \end{vmatrix}. \quad (6)$$

Here, $k_0 = \omega\sqrt{\varepsilon_0 \mu_0}$, $k_c = \omega\sqrt{\varepsilon_{\mathrm{V,G}}\varepsilon_0\mu_0} = k_0\sqrt{\varepsilon_{\mathrm{V,G}}}$ and $k = \omega\sqrt{\varepsilon\varepsilon_0\mu_0} = k_0\sqrt{\varepsilon}$ are wavenumbers in free-space, the shell, and the concealed object respectively, and ε_0 and μ_0 are the permittivity and permeability in free-space. The other determinant V_n^{TM} is obtained by replacing $j_n(.)$ by $y_n(.)$ in the last column of U_n^{TM}. Expressions of determinants U_n^{TE} and V_n^{TE} associated with the nth electrical multipole coefficient are obtained by substituting ε with μ in expressions of U_n^{TM} and V_n^{TM}. It should be noted here that one can derive from Eqs. (5) and (6) that the amplitudes of c_n^{TE} and c_n^{TM} scale with $o(k_0 a_c)^{2n+1}$. This fact makes it clear that, depending on the electrical size of the structure characterized with $k_0 a_c$, only some of these coefficients dominate the total response. The visibility of any object to electromagnetic waves is quantitatively described by its scattering cross section σ_S

$$\sigma_S = \frac{2\pi}{|k_0|^2}\sum_{n=1}^{\infty}(2n+1)\left[\left|c_n^{\mathrm{TE}}\right|^2 + \left|c_n^{\mathrm{TM}}\right|^2\right]. \quad (7)$$

Minimizing σ_S is a *sine-qua-non* condition for invisibility (or transparency). If the quasistatic condition $a_c \ll \lambda$ is satisfied, then cancelling the first term ($n=1$) in the multipole expansion, which is directly related to the integral of the polarization vector of the material $\boldsymbol{P} = (\varepsilon - \varepsilon_0)\boldsymbol{E}$, is already sufficient to greatly reduce σ_S. Under this condition, one can simplify Eq. (7) to $\sigma_S \approx 2\pi/|k_0|^2\,3\left|c_n^{\mathrm{TM}}\right|^2 = (6\pi/|k_0|^2)(k_0 a_c)^3 f_n^2(\gamma)$. Here, $f_n(.)$ are positively valued functions and the ratio $\gamma = a/a_c$ must satisfy the condition:

$$\gamma^3 = \frac{\left[\varepsilon_{\mathrm{V,G}}(\omega) - \varepsilon_0\right]\left[2\varepsilon_{\mathrm{V,G}}(\omega) + \varepsilon\right]}{\left[\varepsilon_{\mathrm{V,G}}(\omega) - \varepsilon\right]\left[2\varepsilon_{\mathrm{V,G}}(\omega) + \varepsilon_0\right]}. \quad (8)$$

Within the frequency band of interest (which is below the interband transition threshold), $\hbar\omega < 2|\mu_c|$ and $|\mu_c| \gg k_B T$ hold true. Therefore, in Eq. (8), the permittivity of graphene $\varepsilon_{V,G}$ can accurately be simplified as $\varepsilon_{\mathrm{V,G}} \approx 1 + j\,\sigma_{\mathrm{intra}}/\delta\varepsilon_0\omega \approx -\omega_{\mathrm{G,p}}^2/\omega(\omega + j\Gamma_c/\hbar)$ where $\omega_{\mathrm{G,p}} = \sqrt{q^2\mu_c/\delta\varepsilon_0\pi\hbar^2}$ is the effective plasma frequency of the graphene layer. Equation (8) is satisfied for two different situations corresponding to negative and close-to-zero but positive values of the complex permittivity $\varepsilon_{\mathrm{V,G}}$; these are denoted with $\varepsilon_{\mathrm{V,G}}^-$ and $\varepsilon_{\mathrm{V,G}}^0$. Figure 2(a) plots the scattering efficiency $\sigma_{\mathrm{S,N}}$ (σ_S normalized by the scattering cross section of the bare dielectric sphere) for a graphene shell with $a_c = 101\,\mathrm{nm}$ and complex permittivity $\varepsilon_{\mathrm{V,G}}^-$ computed for various values of chemical potential μ_c between $100\,\mathrm{meV}$ to $1200\,\mathrm{meV}$, which conceals a dielectric sphere with $a = 100\,\mathrm{nm}$ and $\varepsilon = 3$. Figure 2(b) plots $\sigma_{\mathrm{S,N}}$ of the same structure, where now the complex permittivity of the graphene shell is given by $\varepsilon_{\mathrm{V,G}}^0$

computed for the same values of Γ_c and μ_c. It is clearly shown in these figures that a tunable cloak is designed. Note that $\sigma_{S,N}$ obtained for the shell with $\varepsilon_{V,G}^0$ is more sensitive to the variations in μ_c: When μ_c varies from $500\,\text{meV}$ to $1200\,\text{meV}$, the dip of $\sigma_{S,N}$ moves from $200\,\text{THz}$ to $500\,\text{THz}$ while for $\sigma_{S,N}$ obtained for the design with $\varepsilon_{V,G}^-$ the dip moves only from $40\,\text{THz}$ to $70\,\text{THz}$. On the other hand, the design with $\varepsilon_{V,G}^-$ is a better cloak than the one with $\varepsilon_{V,G}^0$: $\sigma_{S,N}$ of the cloak with $\varepsilon_{V,G}^-$ reaches as low as $30\,\text{dB}$ while that of the cloak with $\varepsilon_{V,G}^0$ saturates at around $10\,\text{dB}$. This is firstly due to lower factor of merit in the latter case ($\text{Re}[\varepsilon_{V,G}^0] \approx \text{Im}[\varepsilon_{V,G}^0]$). Secondly, the wavelength of excitation is of the same order of the object's dimensions; this results in the excitation of higher order multipoles, which play a role in the scattering response in addition to the dipolar mode [11]. It should be noted also that the efficiency of graphene cloaks in comparison with their classical plasmonic counterparts is drastically enhanced thanks to lower intrinsic losses (higher relaxation times) of graphene. This can be seen in Fig. 2(c), which plots the scattering efficiency $\sigma_{S,N}$ of the same graphene shell with complex permittivity $\varepsilon_{V,G}^-$ computed for $\mu_c = 1000\,\text{meV}$ and various values of Γ_c between $0.2\,\text{meV}$ and $4\,\text{meV}$]. Figure 2(d) plots the scattering efficiency $\sigma_{S,N}$ of the same graphene cloak only with $\Gamma_c = 0.65\,\text{meV}$ when it is treated as a thin layer (configuration assumed throughout the manuscript) and when one uses the paradigm of mantle cloaking introduced in [37]. These two approaches give similar results, although they differ slightly in the super-scattering and cloaking regimes.
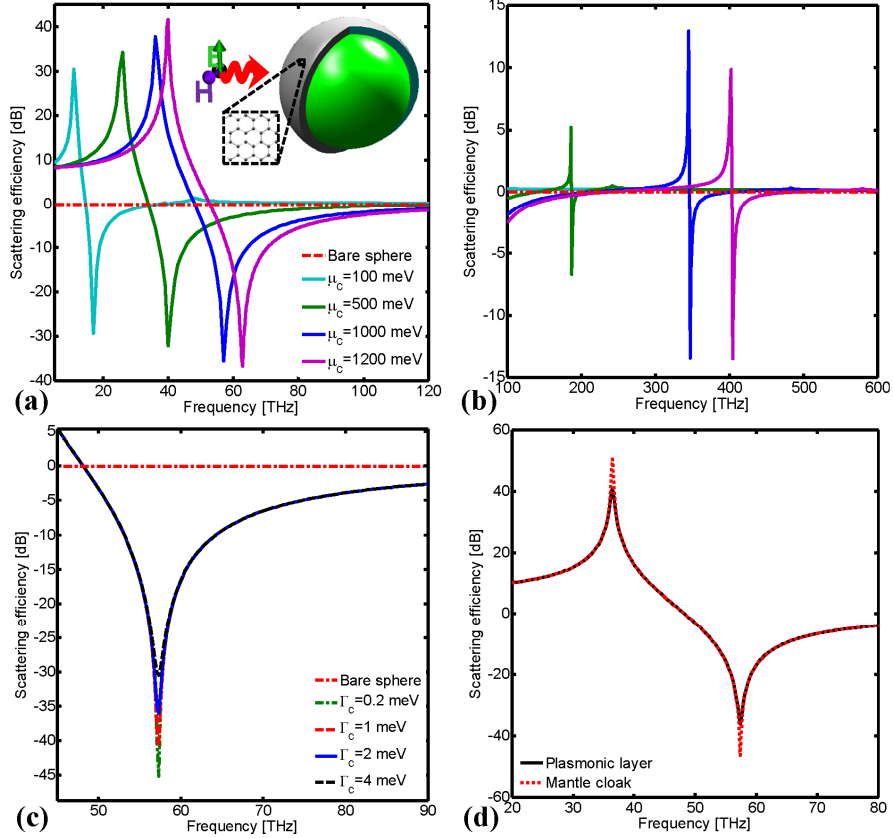
Fig. 2. (a) Scattering efficiency ($\sigma_{\text{S,N}}$) of the dielectric sphere cloaked with the graphene shell with complex permittivity $\varepsilon_{\text{V,G}}^{-}$ (negative solution). $\sigma_{\text{S,N}}$ has dips at various frequencies corresponding to different effective plasma frequencies. (b) Same as in (a) but for the graphene shell with complex permittivity $\varepsilon_{\text{V,G}}^{0}$ (near positive solution). (c) Graphene cloaks with different intrinsic losses for chemical potential 1000 meV. (d) Comparison between graphene plasmonic cloaks and mantle cloaks approximation.

To better illustrate the efficiency of the proposed invisibility cloak, we have computed the electric fields scattered from the cloaked and bare dielectric spheres illuminated by a plane wave with unit amplitude ($1\,\text{V/m}$) electric field in the x-direction and propagating in the y-direction. The frequency of the excitation is 58 THz. Figure 3 shows the amplitude of the total electric field on the xy plane in the case of (a) the bare dielectric sphere (represented in gray color) and (b) the cloaked sphere (cloaking shell is represented in black color). One can clearly see that the total field is less disturbed when the sphere is concealed using the proposed cloak. Uniform amplitude of the total field is restored all around the cloak as if it would propagate in a medium without the scatterer. This confirms the effectiveness of the proposed cloak. In Figs. 3(c) and 3(d) the far-field scattering patterns on the xy plane are provided: It is clearly shown that the cloaked sphere is almost undetectable in the far-field at all angles. The amplitudes of the far-fields scattered from the cloaked sphere are orders of magnitude lower than those of the fields scattered from the bare sphere. Note that the polar axis scales in Figs. 3(c) and 3(d) are different.
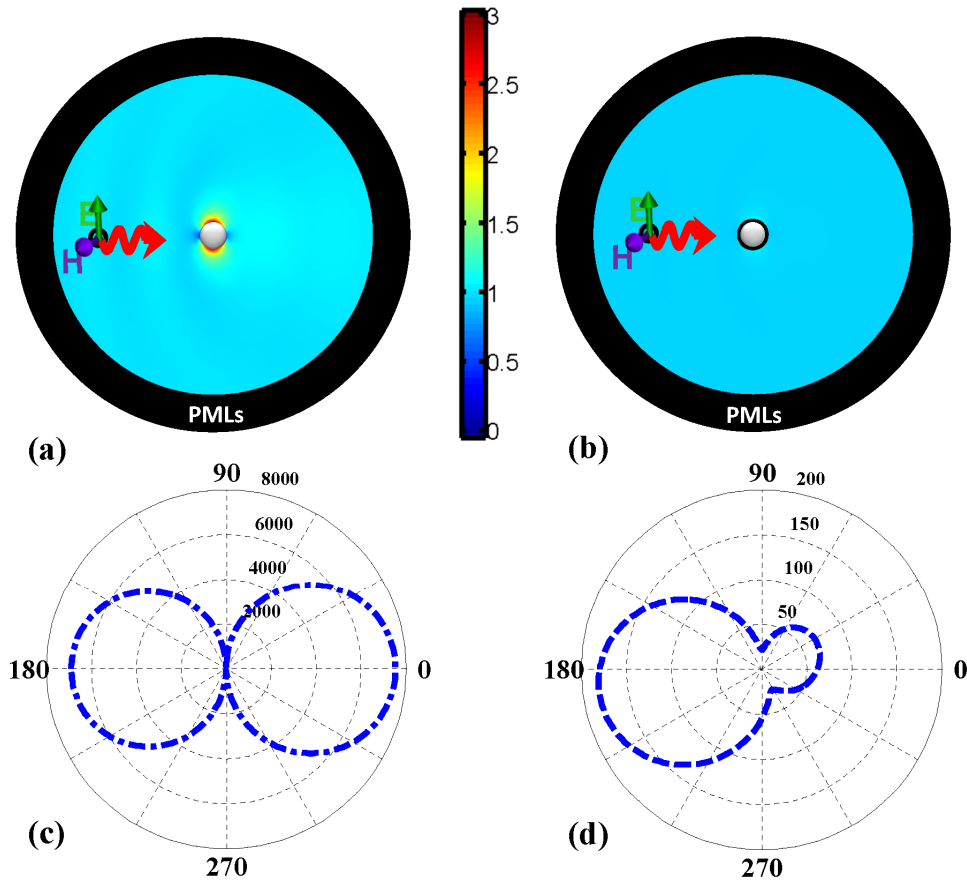
Fig. 3. Norm of the total electric field in V/m in linear scale in the presence of (a) the bare dielectric sphere and (b) cloaked sphere, both illuminated by a plane wave with unit amplitude (1 V/m) electric field in the x-direction and propagating in the y-direction. The excitation frequency is $58\,\text{THz}$. Scattering cross section σ_S normalized by the geometrical cross section πa^2 in linear scale for (c) the bare dielectric sphere and (d) the cloaked sphere on the xy-plane. The scattering form the cloaked sphere is approximately 40 times smaller than the scattering from the bare sphere. Note that the polar axis scales in (c) and (d) are different.

3.2 Multi-frequency multi-layered cloak

In this section, a cloak with multi-band frequency of operation, which is built upon the design of the tunable plasmonic SCT-based cloak described in the previous section, is proposed. For cloaks exploiting SCT, multi-frequency band of operation can be achieved by designing a shell with many layers. Then the complex permittivity of each layer can be obtained by solving a more complex version of Eq. (8) as described in [38]. The challenge in this approach is to find materials with permittivity that would match the solution. Drude materials are prime candidates for this job [37], however it is difficult to find in nature such materials with low loss and plasma frequencies of the same order. Moreover, it would be technically a complex task to build a device made of different materials. Recent developments in graphene manufacturing and wrapping [15,30,32] suggest that such multi-layered cloaks can be constructed using graphene layers biased with different gate voltages.
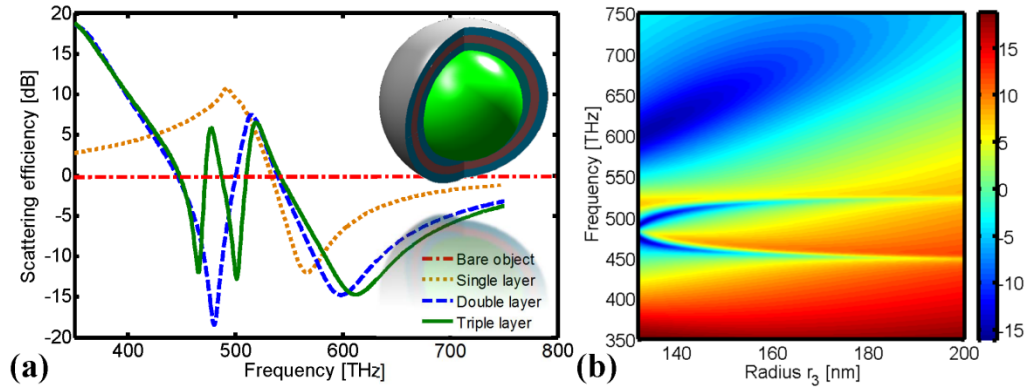
Fig. 4. (a) Scattering efficiency ($\sigma_{S,N}$) for the dielectric sphere of Fig. 2 (dotted-dashed red line) covered by one graphene layer (dotted-red line), two layers (dashed-blue line), and three layers (solid-green line). (b) Scattering efficiency as function of frequency and radius of the third layer in logarithmic scale (in dB).

The capability to individually tune each layer's complex permittivity permits accurate realization of the theoretically predicted values. The resulting cloak suppresses simultaneously the scattering from the object at as many frequencies as the number of shells. This is demonstrated in Fig. 4(a). The figure compares the scattering efficiency of the dielectric sphere (same as the one in the previous section) concealed using cloaks made of one, two, and three layers. A single, double, and triple layers cloak [schematized in the inset of Fig. 4(a)] are biased with chemical potentials $\mu_{c,i} = 900, 700,$ and $500 \, \text{meV}$. The corresponding plasma frequencies are $\omega_{p,i} = 536, 475,$ and $429 \, \text{THz}$ and their radii are $107.5, 131.5,$ and $140 \, \text{nm}$ respectively. The space between any two graphene layers is filled with a dielectric material of permittivity 2.1 . Figure 4(a) clearly shows the scattering reduction at the predicted distinct frequencies; with three layers we observe already the expected three dips of cloaking preceded each by a sharp peak corresponding to the annihilation of coefficient $V_n^{\text{TE,TM}}$ in Eq. (5). The third dip around $60 \, \text{THz}$ is the broadest one. In Fig. 4(b), we analyze in addition the effect of changing the radius of the third layer and the frequency of operation, and it could be observed that increasing it leads to a blue-shift of the third cloaking dip and that after some value around 170 nm, this dip disappear completely.

4. Summary

We describe realistic graphene-based cloaks to conceal three-dimensional objects by suppressing their dipolar scattering at different tunable frequencies (band of frequencies). The proposed cloaking mechanism exploits the fact that graphene layers behave like metals at THz regime with a tunable optical response. It is demonstrated that a cloak, which achieves transparency at a tunable frequency, can be designed with only one graphene shell whose chemical potential can be varied by applying a gate voltage. Based on the same idea, utilizing multiple number of graphene shells biased at different gate voltages results in a cloak that operates at a tunable band of frequencies. We can thus solve one of the most challenging problems of metamaterial cloaks: The limitation on the operation band. One may envision that designs proposed in this work, which exploit tunable electrical properties of graphene, may further render the cloaking theory closer to its practical and feasible realization at optical and THz frequencies. We believe that our results can be easily implemented within an experimental setup. This metamaterial cloak may therefore also represent a viable way for non-invasive sensing and probing with improved bandwidth.